JOURNAL OF AIRCRAFT
Vol. 40, No. 5, September–October 2003

Rotor-Wake Modeling for Simulation of Helicopter Flight Mechanics in Autorotation

S. S. Houston*
University of Glasgow, Glasgow, Scotland G12 8QQ, United Kingdom
and
R. E. Brown†
Imperial College of Science, Technology and Medicine, London, England SW7 2BY, United Kingdom

Rotorcraft flight mechanics simulations typically use finite-state induced velocity models to mimic the effect of the rotor wake on blade loads. However, with recent developments in computational methods coupled flight mechanics and comprehensive rotor-wake analyses have become more tractable. This paper compares results from a finite-state induced velocity model with a vorticity transport wake model that computes the flowfield in a domain around the aircraft. The study focuses on flight mechanics in autorotation. Simple parameter estimation using three- and five-state induced velocity model structures facilitates interpretation of the vorticity transport induced velocity field as well as providing a direct comparison with the finite-state model. Comparisons of performance, trim, and control response indicate that there is little difference between the two models where the autorotative descent is shallow. However, as airspeed reduces the descent angle steepens, and clear discrepancies become apparent. These are directly related to a single parameter in the finite-state model. It is concluded that finite-state models are adequate for much of the autorotation regime, but for low speeds in steep descents the improved resolution of the rotor inflow provided by more comprehensive rotor-wake models might be essential.

Nomenclature

A	=	matrix of state vector acceleration coefficients; linearized model system matrix
A_{11}, etc.	=	minors of linearized system matrix A
B	=	linearized model control matrix
B_1, B_2	=	minors of linearized control matrix B
C_0	=	apparent mass factor
D	=	blade-element drag, N
L	=	blade-element lift, N
$[L]$	=	dynamic inflow static gain matrix
L_{aero}	=	aerodynamic rolling moment, Nm
M_{aero}	=	aerodynamic pitching moment, Nm
p, q, r	=	perturbed angular velocity components about body axes, rad/s
R	=	rotor radius, m
r	=	radial position on rotor disc, m
S	=	source of vorticity
T_{aero}	=	aerodynamic thrust, N
U_p, U_t	=	blade-element velocities, m/s
u, v, w	=	perturbed translational velocity components, body axes, m/s
$\boldsymbol{u}$	=	control vector
$u_{\text{hub}}, v_{\text{hub}}, w_{\text{hub}}$	=	rotor hub velocities in nonrotating reference frame, m/s
V	=	fluid domain
V_x	=	horizontal component of airspeed, kn
V_y	=	vertical component of airspeed, ft/min
$v_i(r, \psi)$	=	induced velocity at position (r, ψ), m/s
v_{i_h}	=	hover value of momentum induced velocity, m/s
v_{i_m}	=	momentum induced velocity, m/s
$v_{i_0}, v_{1_s}, v_{1_c}$	=	components of induced velocity normal to rotor disc, positive down, m/s
v_m	=	wake mass flow velocity, m/s
v_T	=	wake velocity, m/s
$\boldsymbol{x}$	=	state vector
x_{blade}	=	blade Ox axis (positive in direction of rotation)
$\boldsymbol{x}_1, \boldsymbol{x}_2$	=	subspace of linearized model state vector
γ	=	flight-path angle, deg
θ	=	perturbed pitch attitude, rad
$\theta_0, \theta_{0\text{tr}}$	=	perturbed main and tail rotor collective pitch, rad
θ_{1s}, θ_{1c}	=	perturbed longitudinal and lateral cyclic, rad
ν	=	flow velocity, m/s
ρ	=	air density, kg/m^3
$[\tau]$	=	time constant matrix, s
ϕ	=	perturbed roll attitude, rad; inflow angle $[\tan^{-1}(U_p/U_t)]$, rad
χ	=	wake skew angle, rad
ψ	=	azimuthal position on rotor disc (zero to rear), rad; perturbed yaw attitude, rad
ω	=	vorticity

Subscript

wind	=	wind axes

Received 31 March 2002; revision received 28 February 2003; accepted for publication 15 March 2003.

*Senior Lecturer, Department of Aerospace Engineering. Member AIAA.
†Lecturer, Department of Aeronautics.

Introduction

ROTORCRAFT mathematical modeling for stability, control, and handling qualities applications has developed steadily to address deficiencies in fidelity that have been identified by validation against test data. Developments have generally followed the path of increasing complexity and comprehensiveness, typically by increasing the degrees of freedom in the model structure.[1] For example, modeling of the main rotor has progressed from disc representations, whose behavior was considered to be quasi-steady, to formulations with individual blade dynamics driven by loads summed over a number of elements. An important element of these models is the representation of the rotor wake, but here the model structure has remained fairly simple over the years, with so-called finite-state

induced velocity models being used to mimic the effect of the rotor wake on blade loads. Gaonkar and Peters[2] is preeminent in this field, and many coworkers have ensured that developments continue to address issues in rotorcraft flight mechanics, for example, Ref. 3. Chen[4] conducted a thorough review of finite-state wake modeling.

The finite-state model benefits from a rigorous theoretical development that results in an elegant and computationally efficient formulation. Sophisticated and comprehensive wake models, providing very high resolution of real flowfield features, are generally the domain of performance and airload calculations. However, recent developments in computational methods allow flight mechanics and better rotor-wake methods to be coupled. Although computationally demanding, a wake code allows the impact of real flowfield features on flight mechanics to be quantified. For example, a range of blade/blade, main/tail rotor, and rotor/airframe interactions can be investigated. A number of approaches to the problem of a wake code suitable for flight mechanics studies exist, for example, Refs. 5–7. Brown's CFD-type approach to modeling vorticity transport in the wake takes particular care to control dissipation of vortical structures.[5] Theodore and Celi[6] take a different approach, using a weakly time-dependent free-wake code. Leishman[7] has surveyed contemporary developments in numerical methods for wake codes.

The aim of this study is to explore vorticity transport and finite-state induced velocity models in autorotation for use in typical flight mechanics calculations such as trim, performance, and control response. The objectives are as follows: first to determine if ambiguities exist questioning the legitimacy of either model in autorotation; second, to identify if equivalent finite-state modes exist in the induced velocity field of the vorticity transport wake model, thereby guiding selection of the appropriate number of modes in a finite-state model; and finally, to determine if features in the complex flowfield of the vorticity transport model have a role to play in helicopter flight mechanics in autorotation. Although comparison of induced velocity distributions calculated using finite-state and wake codes has been made previously in Ref. 4, little emphasis has been placed on their relative impact on vehicle flight mechanics, that is, trim, performance, and control response, for example, Ref. 8. Finally, the topic of helicopter flight mechanics in autorotation has received only scant attention in the literature,[9,10] and so this paper strives to make a contribution in a number of interrelated areas.

Background

Autorotation is an abnormal mode of operation for a helicopter because no powerplant torque is applied to the main rotor, requiring descending flight to provide an upward flow of air through the rotor to sustain rotation and hence lift. Failure of the helicopter's powerplant, or a tail rotor failure, requires the aircraft to enter autorotation in order that a safe descent and landing can be effected. Figure 1 shows a schematic of the arrangement of blade element lift and drag forces in autorotation, clearly illustrating the need for upward flow of air to sustain rotor rotation. Autorotation is flown with the main rotor blade collective pitch control either at, or close to, its minimum

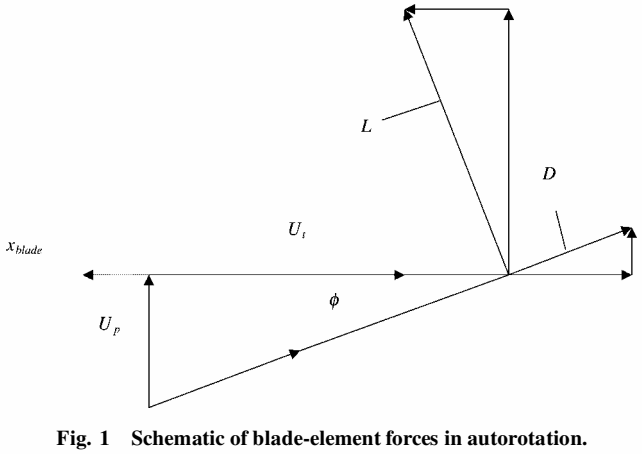

Fig. 1 Schematic of blade-element forces in autorotation.

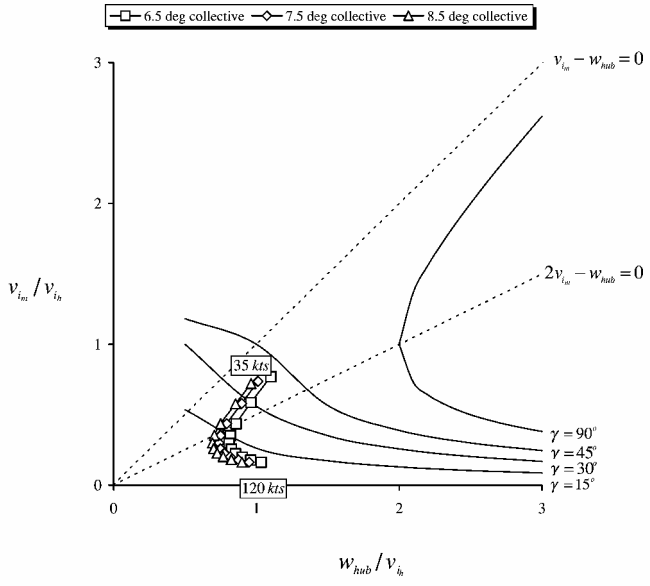

Fig. 2 Comparison of simulations with momentum theory solutions and limitations.

value and the range of movement is a fraction of that available in powered flight because of the need to keep the rotor speed within limits. Autorotation then effectively defines a flight envelope boundary with glide performance curves similar in appearance to those for an airplane. Although contemporary rotorcraft mathematical models can in principle simulate autorotation, modeling of induced velocity (which can be a significant and therefore important contribution to U_p) is normally based on momentum principles, requiring care in application caused by the ambiguity in clearly defining a control volume in the autorotative state. Figure 2 illustrates momentum theory solutions for a range of flight-path angles together with simulation results used as the basis for this paper. The two boundaries delimit flow state changes in axial flight and hence regions of nonviable momentum solutions. For example, $2v_{i_m} - w_{\text{hub}} = 0$ represents solutions for which no well-defined slipstream exists in the developed wake because the induced velocity exceeds the descent rate; $v_{i_m} - w_{\text{hub}} = 0$ represents solutions for which there is no net flow through the rotor and again a well-defined slipstream does not exist. This diagram is usually only viewed in the context of axial flight, and care is required when interpreting the forward flight solutions and simulation cases in this context.

The vorticity transport wake model is an alternative means of calculating the induced velocity and has been compared with a three-state induced velocity model[8] in power-on level flight. Validation against a comprehensive flight-test database between hover and high speed suggested that the vorticity transport model offered improved prediction of cross coupling and better representation of vibration. In the calculation of trim, both models gave very similar predictions of airframe attitude and main rotor control angles, and only in respect of tail rotor collective pitch did the vorticity transport model confer improved correlation with flight data. However for autorotation, helicopter validation data are not available—standard model validation inputs such as frequency sweeps and multi-teps conducted at what is essentially the limit of the flight envelope are arguably a challenge to safety of flight. For example, the rotor speed can be at maximum or minimum limits, and height loss during a typical frequency sweep could be anywhere between 2000–5000 ft. However, for autogyros, flight in sustained autorotation is a benign normal operation, and it can be argued that they offer a viable alternative for generically validating a flight mechanics model in autorotation before it can be applied to the helicopter problem with a degree of confidence. An important precursor to the helicopter case has therefore been extensive validation against two dissimilar autogyro types,[11,12] although these studies have used only the three-state induced velocity model.

Autorotation is therefore an important mode of helicopter operation, as it constitutes a flight envelope boundary. Simulation is

challenged by application to such a regime but can enhance analysis, the design process, and hence flight safety. Finite-state induced velocity modeling is arguably of questionable validity in descents such as autorotation, and the vorticity transport model provides an opportunity to explore this aspect from an alternative standpoint. In particular, the wake skew angle behavior in descents such as autorotation can influence terms in the finite-state model quite differently from a corresponding power-on flight condition.[4,10]

Mathematical Modeling

Finite-State Dynamic Inflow Model

The dynamic inflow representation used is taken from Chen,[4] although the original model development is from Gaonkar and Peters[2] and Peters and HaQuang.[13] The basic form of induced velocity at any azimuth and radial station over the rotor is given by

$$v_i(r,\psi) = v_{i_0} + \frac{r}{R}\left(\sum_{k=1}^{n} v_{k_s}\sin k\psi + \sum_{k=1}^{n} v_{k_c}\cos k\psi\right) \tag{1}$$

The induced velocity $v_i(r,\psi)$ appears explicitly in the aerodynamic model, contributing to the blade-element angle of attack. It is common to consider the case with $n=1$. The three states v_{i_0}, v_{1_s}, and v_{1_c} are calculated from

$$[\tau]\begin{bmatrix}\dot{v}_{i_0}\\ \dot{v}_{1_s}\\ \dot{v}_{1_c}\end{bmatrix}_{\text{wind}} = -\begin{bmatrix}v_{i_0}\\ v_{1_s}\\ v_{1_c}\end{bmatrix}_{\text{wind}} + [L]\begin{bmatrix}T_{\text{aero}}\\ L_{\text{aero}}\\ M_{\text{aero}}\end{bmatrix}_{\text{wind}} \tag{2}$$

where

$$[\tau] = \begin{bmatrix} \dfrac{4R}{3\pi v_T C_0} & 0 & \dfrac{-R\tan(\chi/2)}{12 v_m} \\ 0 & \dfrac{64R}{45\pi v_m(1+\cos\chi)} & 0 \\ \dfrac{5R\tan(\chi/2)}{8 v_T} & 0 & \dfrac{64R\cos\chi}{45\pi v_m(1+\cos\chi)} \end{bmatrix} \tag{3}$$

and

$$L = \frac{1}{\rho\pi R^3}\begin{bmatrix} \dfrac{R}{2v_T} & 0 & \dfrac{15\pi\tan(\chi/2)}{64 v_m} \\ 0 & \dfrac{-4}{v_m(1+\cos\chi)} & 0 \\ \dfrac{15\pi\tan(\chi/2)}{64 v_T} & 0 & \dfrac{-4\cos\chi}{v_m(1+\cos\chi)} \end{bmatrix} \tag{4}$$

Equation (2) is transformed from wind to body axes in this application. The time constant and static gain matrices [Eq. (3) and (4) respectively] have their origin in a combination of the apparent air mass concept and a vortex cylinder model. The wake skew angle is given by

$$\tan\chi = \frac{\sqrt{u_{\text{hub}}^2 + v_{\text{hub}}^2}}{v_{i_{0m}} - w_{\text{hub}}} \tag{5}$$

which differs from Peters' definition.[13] If $v_{i_{0m}} - w_{\text{hub}} > 0$, for example, in level or climbing flight, then $0 \text{ deg} \le \chi < 90$ deg. However, in descending flight such as autorotation, $v_{i_{0m}} - w_{\text{hub}} < 0$ and χ then clearly have an important role to play in determining the magnitude of the induced velocity components, because $90 \text{ deg} < \chi \le 180$ deg (Refs. 4 and 10). Of particular interest is the impact on the induced velocity components in steep low-speed descents, for which $\chi \to 180$ deg.

Vorticity Transport Wake Model

A full description of this model is given in Ref. 5, and only an outline is given here. For aeromechanics purposes a straightforward way of constructing a comprehensive model for the aerodynamic environment of the rotor is to represent the wake by a time-dependent vorticity distribution in the region of space surrounding the rotor. If v is the velocity of the flow, then the associated vorticity distribution $\omega = \nabla \times v$ evolves according to the unsteady vorticity transport equation

$$\frac{\partial}{\partial t}\omega + v\cdot\nabla\omega - \omega\cdot\nabla v = S(x) \tag{6}$$

This equation can be derived from the Navier–Stokes equation under the assumption of incompressibility and in the limit of vanishing viscosity[5] and shows the rotor wake to arise as a vorticity source S associated with the generation of aerodynamic loads on the rotor blades. The differential form

$$\nabla^2 v = -\nabla\times\omega \tag{7}$$

of the Biot–Savart law relates the velocity at any point near the rotor to the vorticity distribution in the flow and allows the geometry and strength of the rotor wake to feed back into the aerodynamic loading and the dynamics of the rotor.

The vorticity transport model developed by Brown[5] employs a direct computational solution of Eq. (6) to simulate the evolution of the wake of the helicopter. The model is capable of faithfully representing blade-wake interactions, as well as the wake-wake interactions that lead to the growth, coalescence, and rupture of vortical structures in the rotor wake, and thus embodies a high level of physical realism. This model is coupled into the flight mechanics simulation by using the loads generated by the rotor's lifting-line aerodynamic model to construct S in terms of the shed and trailed vorticity from the blades on each rotor. After casting the equations on a structured computational grid surrounding the rotor, Eq. (7) is solved by cyclic reduction, whereas Eq. (6) is marched through time using Toro's Weighted Average Flux algorithm.[14]

The principal advantage of this method is that it can deal naturally with interactional aerodynamic phenomena. This means that the induced velocity field on the rotor can be so complex as to defy description by Eq. (1). However, simple parameter estimation by regression fit using the finite-state model structure facilitates interpretation of the vorticity transport model and allows direct comparisons to be made.

Nonlinear Model Description

The flight mechanics model is described more fully in Refs. 10, 11, and 15. It is a generic rotorcraft simulation code and takes the form

$$A\dot{\boldsymbol{x}} = f(\boldsymbol{x},\boldsymbol{u}) \tag{8}$$

where the state vector $\boldsymbol{x}$ contains the airframe translational and angular velocity, blade flap, lag and feather angles and rates for each blade on each rotor, the induced velocity states for each rotor wake as well as the angular velocity of both rotors, and the engine torque. Elements of the control vector $\boldsymbol{u}$ are the four controls, which vary with aircraft type, for example, single main and tail rotor configurations will have three main rotor controls and one tail rotor control. Blade attachment is modeled as offset hinges and springs with a linear lag damper. The aerodynamic and inertial loads are represented by up to 20 elements per blade. Rotor blade-element lift and drag forces are functions of section angle of attack and Mach number, derived from two-dimensional look-up tables. Airframe aerodynamic loads are functions of angle of attack and sideslip, also derived from two-dimensional look-up tables. Depending on the number of blades on each rotor, there can be up to 100 nonlinear, periodic ordinary differential equations describing the coupled rotor/airframe behavior. A simple model of the International Standard Atmosphere is used, with provision for variation in sea-level temperature and pressure.

The matrix A contains off-diagonal terms associated with airframe products of inertia, dynamic inflow, and blade equations of motion.

Trim and linearization are performed using the procedure described in Ref. 15. However, autorotation requires the linearization process to reduce the model to the form

$$\begin{bmatrix}\dot{\boldsymbol{x}}_1\\ \dot{\boldsymbol{x}}_2\end{bmatrix} = \begin{bmatrix}A_{11} & A_{12}\\ A_{21} & A_{22}\end{bmatrix}\begin{bmatrix}\boldsymbol{x}_1\\ \boldsymbol{x}_2\end{bmatrix} + \begin{bmatrix}B_1\\ B_2\end{bmatrix}\boldsymbol{u} \tag{9}$$

where the conventional six-degree-of-freedom, nine-state model structure is represented by

$$\dot{\boldsymbol{x}}_1 = A_{11}\boldsymbol{x}_1 + A_{12}\boldsymbol{x}_2 + B_1\boldsymbol{u}, \qquad \boldsymbol{x}_1 = [u, v, w, p, q, r, \phi, \theta, \psi]^T \tag{10}$$

and

$$\dot{\boldsymbol{x}}_2 = A_{21}\boldsymbol{x}_1 + A_{22}\boldsymbol{x}_2 + B_2\boldsymbol{u}, \qquad \boldsymbol{x}_2 = [\Omega] \tag{11}$$

is the rotor-speed degree of freedom. The minor A_{12} then couples rotor speed into the conventional rigid-body degrees of freedom. The treatment of Ω is in accordance with convention for derivative calculation, that is, it is held constant for calculation of elements in A_{11}, A_{21}, B_1, and B_2, and only perturbed for deriving the elements in A_{22} and A_{12}. Reduction of the nonlinear model to the form given by Eq. (10) limits the bandwidth of applicability, because rotor blade dynamics are treated in a quasi-steady manner by the linearization process. This is not regarded as a limitation for parametric studies.

Results

The mathematical model was configured with data to represent the Puma, a medium helicopter with a four-bladed main rotor and a five-bladed tail rotor. The aircraft mass was set at 5600 kg, and the nominal density altitude was 4000 ft. The autorotation flight envelope was defined by a range of steady airspeed and rate of descent combinations that each resulted in a main rotor collective pitch angle of 6.5 deg, just above the minimum for this aircraft of 6 deg. Momentum solutions for forward flight can cross the axial flight developed wake flow boundary ($2v_{im} - w_{\text{hub}} = 0$) even at the relatively shallow descent angle of 15 deg. Figure 2 shows that this occurs at airspeeds below 60 kn for these simulations. Each rotor blade was modeled using 20 elements along its span, and the numerical integration step length was consistent with calculation every 22.5 deg of tail rotor blade azimuth position, or just under 5 deg of main rotor blade azimuth. For a single main and tail rotor helicopter the rotor module is called twice in the simulation code, each rotor being discriminated by data that specify its location and orientation on the airframe and its characteristics in terms of blade mass distribution, hinge offset, and restraint, etc.

Vorticity Transport Model

Figure 3 is a snapshot of the vorticity field in the rotor wake, where the rate of descent is 1800 ft/min at an airspeed of 80 kn. The wake is represented by a surface of constant vorticity magnitude with the threshold set low enough to capture the overall morphology of the wake while suppressing detail. The structure is seen to develop above the rotor as expected in autorotation. Note the roll up of the vorticity on the rotor disc into two trailing vortices in the developed wake. The area between these is relatively smooth and only slightly asymmetric laterally. These results are qualitatively similar to solutions from free-wake models in regard to features such as vortex bundling.

The corresponding induced velocity at each blade element is presented in Fig. 4. Figure 5 shows the regression fits to this surface using three- and five-state model structures. Generally, the three-state structure captures the underlying fundamental shape of the induced velocity field calculated by the vorticity transport model. The addition of the extra degrees of freedom afforded by the five-state structure serves to mimic the presence of the ridge features at 45- and 270-deg azimuth, but fails to capture their radial variation. The inboard blade loading is thus seriously underestimated by three- and five-state structures. This is shown clearly in Fig. 6a; these "ridge" effects on the advancing and retreating sides produce a pronounced

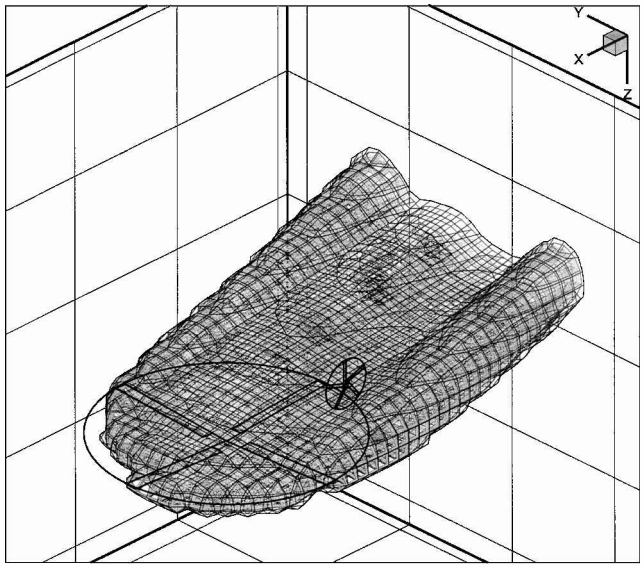

Fig. 3 Wake morphology: airspeed 80 kn and rate of descent 1800 ft/min.

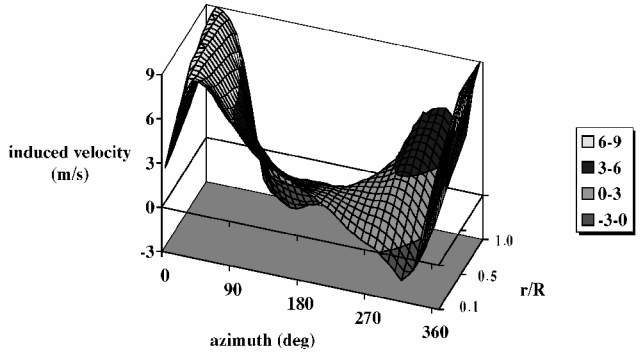

Fig. 4 Induced velocity, vorticity transport model: airspeed 80 kn and rate of descent 1800 ft/min.

inboard once-per-rev variation in induced velocity that simply cannot be matched by a linear variation with radius. However, towards the tip the five-state model structure improves the visual quality of the fit, although a phase lag of around 30 deg in the model structure would improve matters further in this region.

As airspeed increases, the vorticity transport model becomes less easy to describe in terms of a simple finite three or five-state model structure. At low speeds the mismatch errors are an order of magnitude less than the overall level of induced velocity, whereas the error is of the same order as the induced velocity at higher speeds.

Comparison with Finite-State Model Induced Velocity

Figure 7 compares the three-state induced velocity model with the coefficients from the regression fits of the vorticity transport model. For the latter the narrow confidence bounds on v_0 and v_{1c} are indicative of robust estimates of these variables; there is a greater degree of uncertainty in the estimates of v_{1s}.

Correlation between the two models is poor in respect of v_{1s}, but much better for v_0. The v_{1c} results diverge rapidly below about 70 kn. The finite-state induced velocity model displays asymptotic behavior attributed to $\chi \to 180$ deg, as highlighted in Ref. 10, and this precludes solution at very low airspeeds and high rates of descent. In contrast, the vorticity transport model is well behaved. The airspeed trend of the harmonic components identified from the vorticity transport model changes between 20 and 40 kn, consistent with a change in the nature of the flowfield. This is illustrated in Fig. 8, which shows the intermediate morphology between the wing-type wake structures found at speeds above 40 kn, and the stream-tube wake structures associated with a steep low-speed descent.

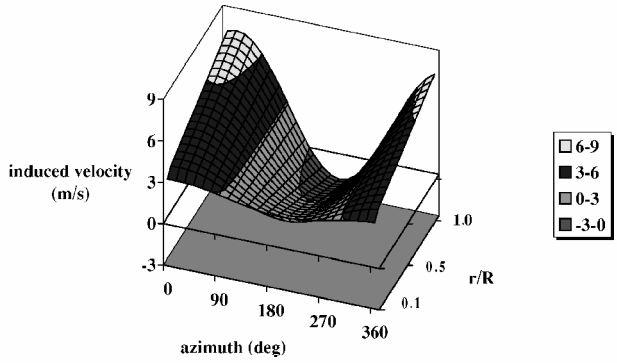

a) Three-state model structure

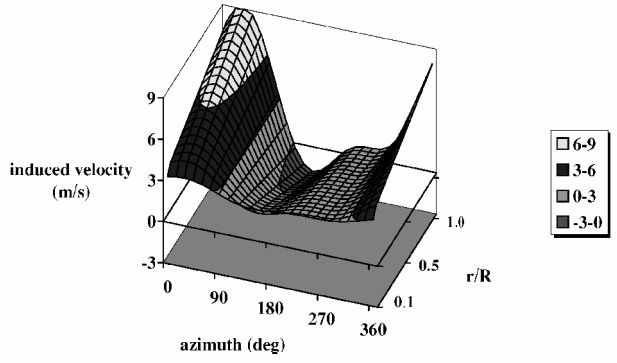

b) Five-state model structure

Fig. 5 Induced velocity regression fits to vorticity transport model: airspeed 80 kn and rate of descent 1800 ft/min.

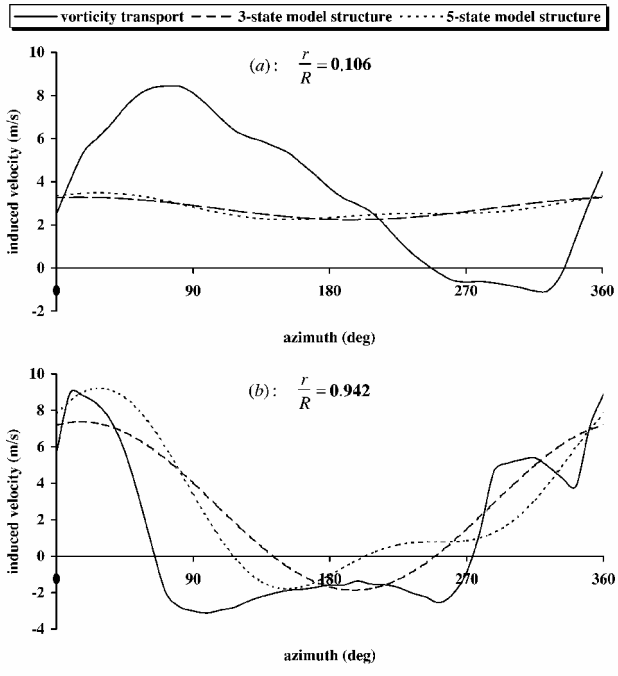

Fig. 6 Induced velocity regression fits: airspeed 80 kn and rate of descent 1800 ft/min.

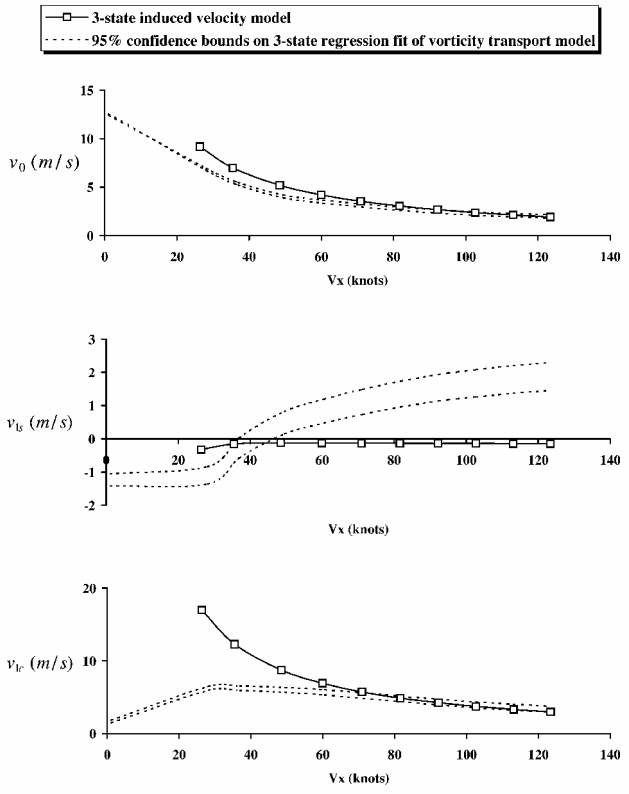

Fig. 7 Comparison of three-state induced velocity components: finite-state and vorticity transport models.

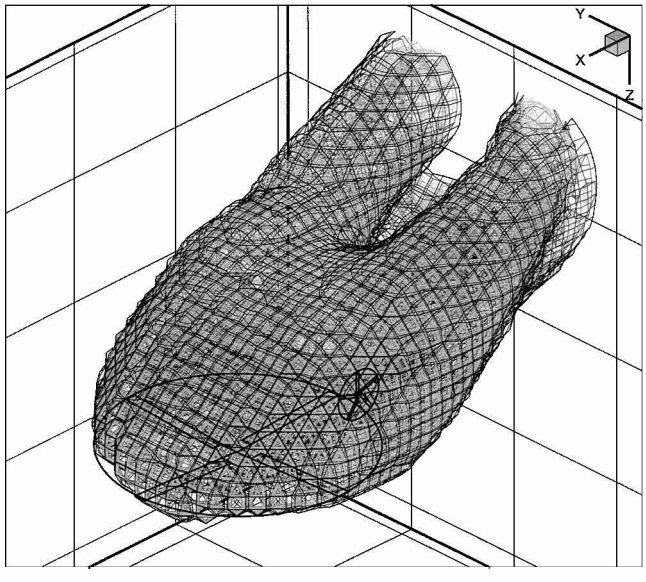

Fig. 8 Wake morphology: airspeed 35 kn and rate of descent 2375 ft/min.

Performance and Trim Comparisons

Figure 9 compares the two models for the calculation of flight-path performance. The vorticity transport wake model gives maximum endurance and range airspeeds some 10–15 kn lower than that using the finite-state induced velocity model, predicting approximately 10% better maximum endurance but 10% worse maximum range.

Figure 10 shows main rotor lateral flapping angle and aircraft roll attitude. These variables are important because they provide an indirect verification of the magnitude of v_{1c} in two ways. First, a large value of v_{1c} will result in significant in-plane rotor side force to the right (balanced by a negative roll attitude in the absence of tail rotor thrust as found in autorotation). Second, for the Puma with its clockwise rotating rotor (viewed from above) v_{1c} gives rise to lateral flapping to the left. It is clear that the roll attitude and lateral flapping trends with airspeed are consistent with the respective variations in v_{1c} shown in Fig. 6.

Figure 10 also shows that the two models trim with increasingly dissimilar rotor speed towards either end of the speed range. For steep flight paths at low speed, the difference can be as much as 2 rad/s, or 20 rpm, reducing to less than half this figure for a shallow high-speed

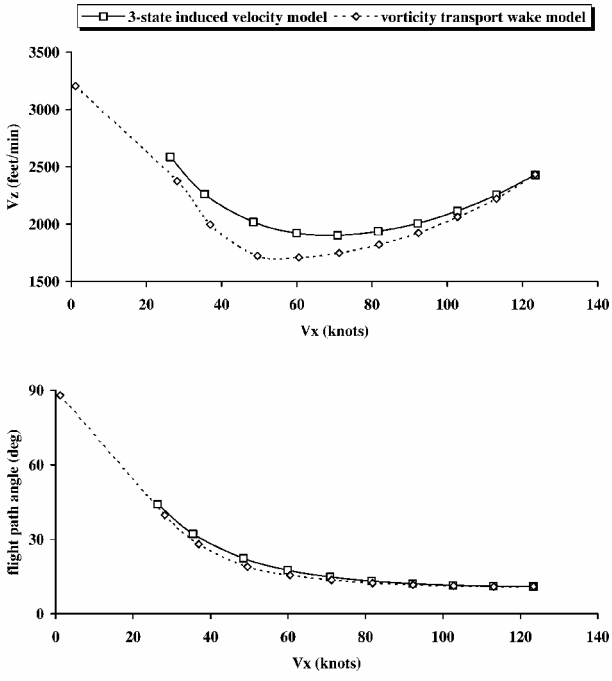

Fig. 9 Comparison of flight-path performance for finite-state and vorticity transport models.

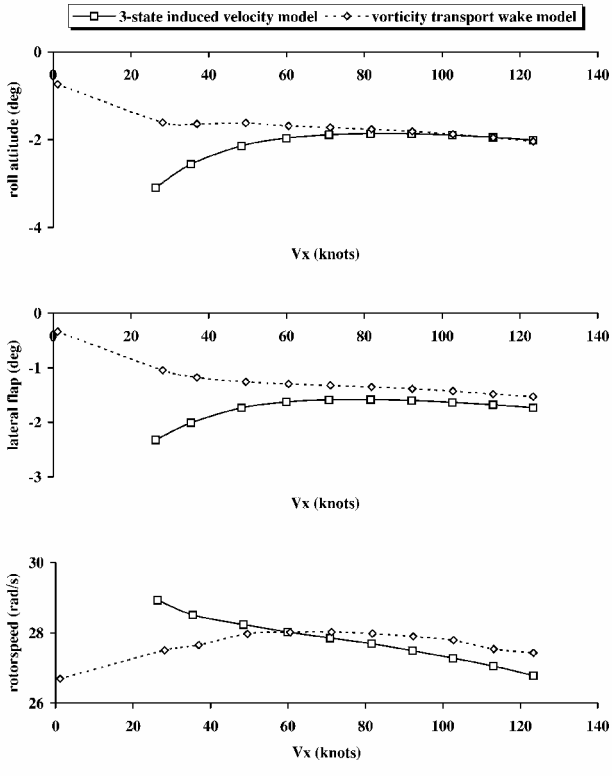

Fig. 10 Trim comparison for finite-state and vorticity transport models.

descent. In Fig. 11 the differences in tail-rotor collective pitch are considerable at both ends of the speed range. This can be attributed to differences between the two models in the calculation of tail-rotor speed: the main and tail rotors are linearly geared; hence, differences in tail rotor angular velocity will be of the same form as that shown for the main rotor in Fig. 10. However, aerodynamic interaction between the main and tail rotors, an effect treated naturally by the vorticity transport formulation but not modeled by the finite-state representation, is also a plausible contributor to this result.[8]

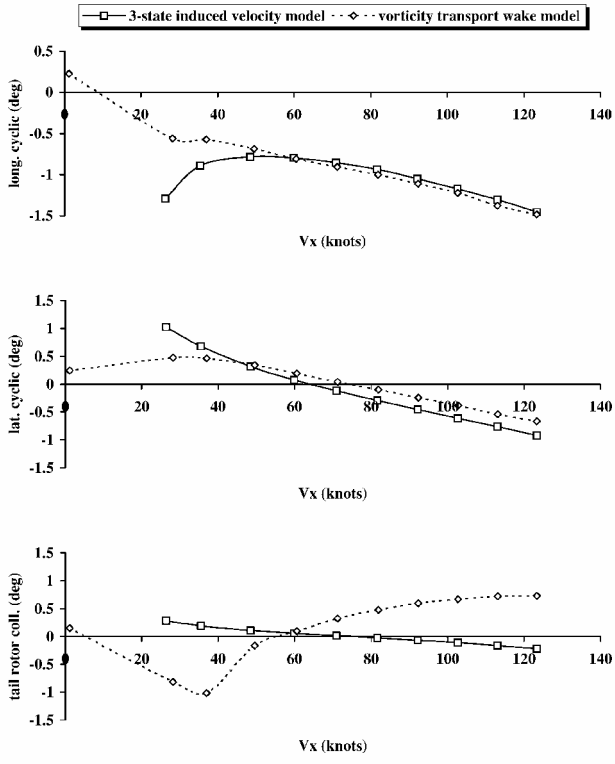

Fig. 11 Comparison of flight controls required to trim finite-state and vorticity transport models.

Finally, comparison of the main rotor cyclic angles required for trim highlights significant discrepancies between the two models below 50 kn (Fig. 11). The lateral cyclic pitch difference can be explained readily as a consequence of the low-speed discrepancy in v_{1c}. However, the longitudinal cyclic pitch mismatch cannot be explained in terms of the relative difference in v_{1s}. Positive static longitudinal stability is a certification requirement for normal and transport category helicopters,[16,17] and so accurate prediction of cyclic position is an important modeling issue. However, the source of the discrepancy is difficult to isolate. The longitudinal cyclic gradient diminishes with reducing airspeed in both cases. This behavior is dominated by the horizontal stabilizer pitching moment. The slope reversal obtained with the finite-state model is a result of horizontal stabilizer stall, and although this is also present with the vorticity transport formulation some other mechanism is responsible for masking the reversal of cyclic gradient. Figure 12 shows that the principal mismatch between the two wake models is inboard, and it might be the case that these induced velocity variations, although inboard, are of sufficient magnitude to influence the longitudinal cyclic position.

Control Response Comparisons

Bode plots allow a broad interpretation of the response to controls and are the basis of defining small-amplitude handling criteria for helicopters.[18] Figures 13 and 14 show representative plots for the upper half of the speed range. There is little difference between the two induced velocity models in terms of attitude response to cyclic, although the vertical velocity and rotor-speed responses to collective pitch differ by about 6 dB in the midfrequency range. However, at low speed (Figs. 15 and 16) large discrepancies between the two models, particularly in the attitude response, raise clear issues of uncertainty in simulation of flight mechanics in autorotation that require further study. As these differences pervade the frequency range, this includes use of the models not just for stability and control studies, but also for handling qualities, which are predicated on the gain and/or phase characteristics approaching crossover, typically around 2–3 rad/s.

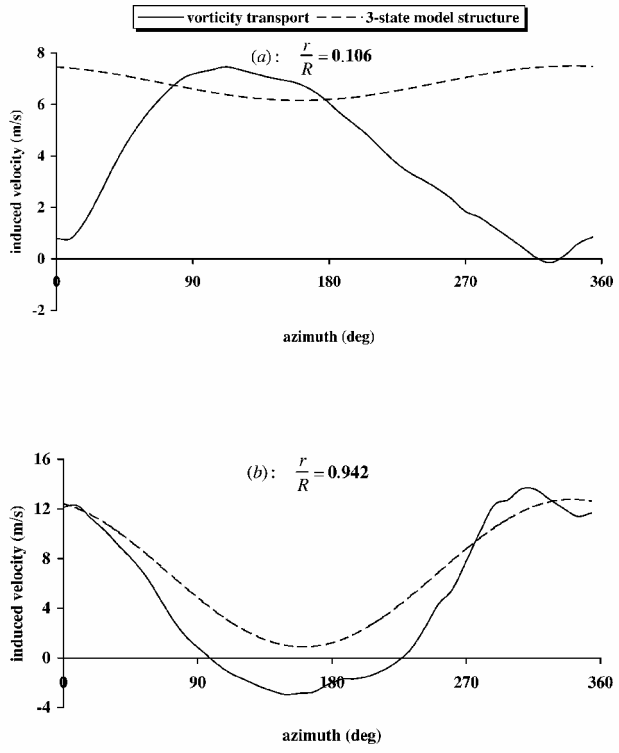

Fig. 12 Induced velocity regression fits: airspeed 35 kn and rate of descent 2375 ft/min.

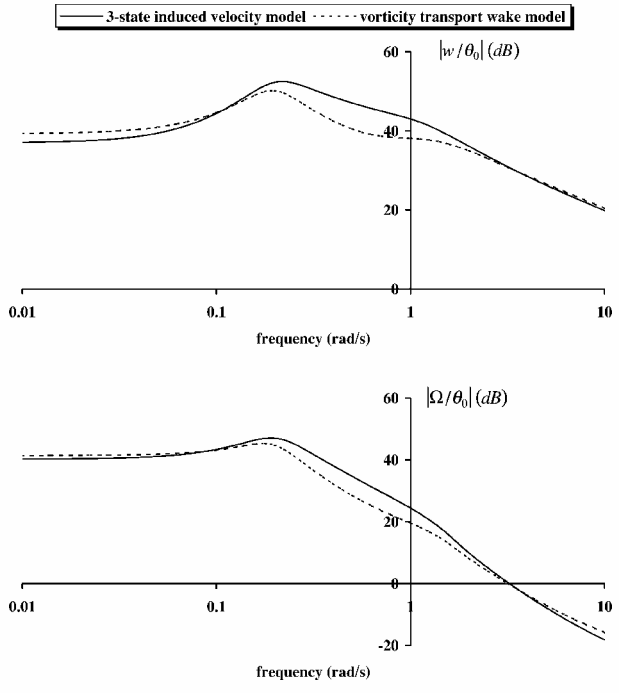

Fig. 13 Finite-state and vorticity transport model comparison: collective pitch frequency responses; airspeed 80 kn.

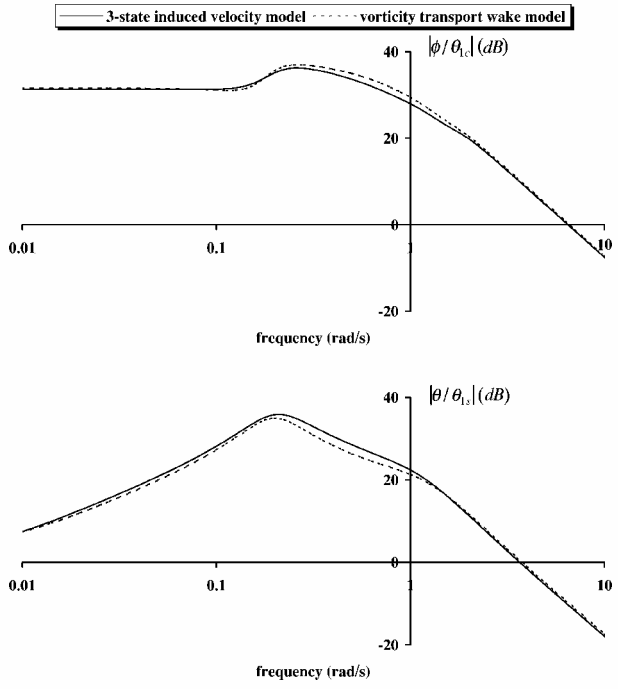

Fig. 14 Finite-state and vorticity transport model comparison: cyclic pitch frequency responses; airspeed 80 kn.

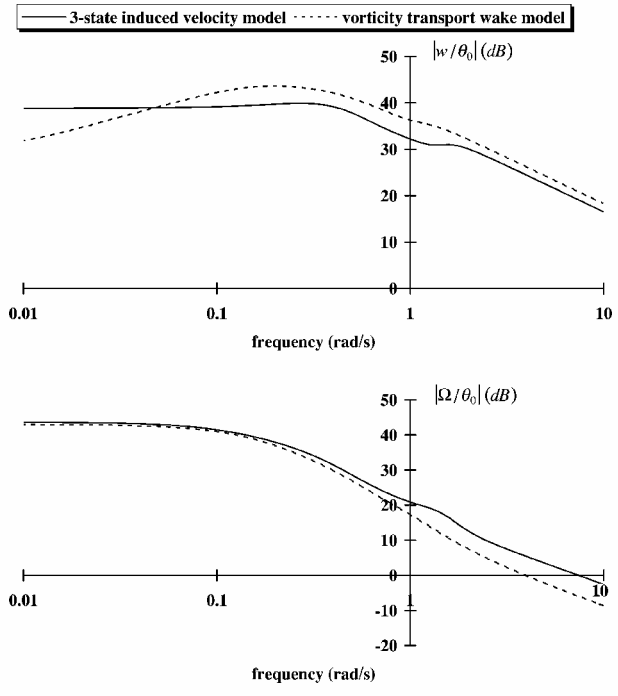

Fig. 15 Finite-state and vorticity transport model comparison: collective pitch frequency responses; airspeed 35 kn.

Discussion

In the upper half of the speed range, description of the vorticity transport wake model in terms of the finite-state model structure is challenged because of real flowfield features such as blade-vortex interactions. The finite-state induced velocity model can, in principle, simulate these characteristics by the addition of higher modes. However, because the two wake models give very similar comparisons of trim, performance, and control response in this regime these phenomena might have little impact on flight mechanics in autorotation. Use of a three-state induced velocity model might be appropriate, and this is consistent with other studies that report ambiguity with regard to the significance of higher induced velocity modes in helicopter flight mechanics modeling (e.g., Ref. 19). For the finite-state induced velocity model rapidly increasing v_{1c} with reducing airspeed is a direct consequence of wake skew angle behavior in the steep descents found at low airspeeds. This characteristic is absent with the vorticity transport formulation, which could be trimmed in a very steep autorotative descent where the finite state model could not. Arguably, this result is of little consequence, as such flight paths are of limited practical use to pilots. However, such paths are aeromechanically viable, and, unless artificially prohibited by

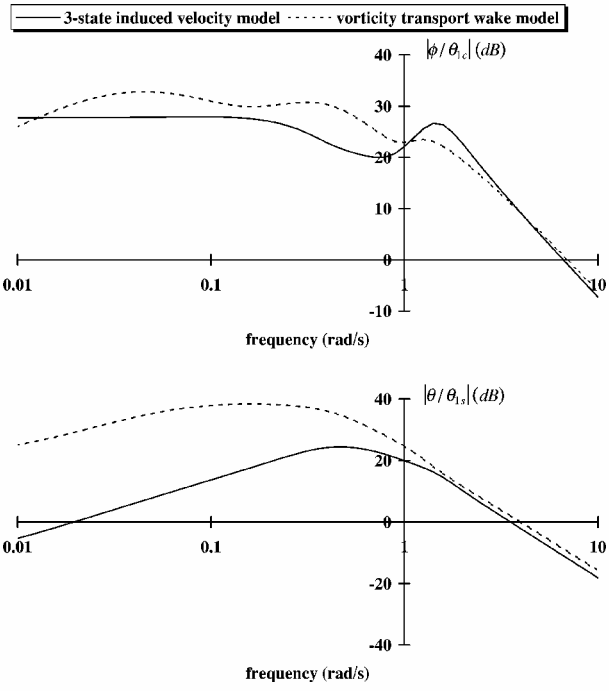

Fig. 16 Finite-state and vorticity transport model comparison: cyclic pitch frequency responses; airspeed 35 kn.

limitations in the flight manual, it is conceivable that the helicopter could be flown in this area where the modeling results are ambiguous. Validation against flight-test data would serve to resolve this ambiguity. Although v_{1c} cannot be directly measured, either main rotor lateral flapping angle or roll attitude could be used as indirect indicators of the magnitude of the effective v_{1c}.

There is a high computational price to pay for use of the vorticity transport wake model in flight mechanics applications. A model of this complexity might however prove to be necessary for simulation of a steep low-speed autorotative descent. At higher speeds the two approaches are convergent, although the wake model's treatment of interactional aerodynamics can have some bearing on the tail-rotor collective pitch angle. The role of the vorticity transport model in this case might be to serve as a guide to the modes that need to be incorporated to exploit the elegant formulation and computational efficiency of the finite-state approach.

Conclusions

The induced velocity distribution derived from a complex flowfield simulation such as the vorticity transport wake model has been categorized in terms of a finite-state induced velocity model structure to allow direct comparison of the two modeling approaches. As airspeed reduces, the descent angle becomes steeper, and the finite-state formulation displays rapidly increasing longitudinal variation of induced velocity, which is attributed directly to the behavior of terms associated with the wake skew angle. There is a clear discrepancy with the vorticity transport wake model in this part of the flight envelope, and, as a result, performance trim, and control response comparisons are consistently dissimilar. However both models present very similar results in the upper half of the speed range, where the descent angle is relatively shallow and the overall magnitude of the induced velocity is much less. The natural advantages of the finite-state model are elegant formulation and computational efficiency, but it is concluded that they cannot be exploited in the simulation of helicopter flight mechanics in autorotation without further study to resolve the discrepancies with the vorticity transport wake model in steep low-speed descents. There is a strong need for validation against flight-test data before the finite-state approach can be used with confidence to model helicopter behavior in steep low-speed autorotative descents.

References

[1]Padfield, G. D., *Helicopter Flight Dynamics*, Blackwell Science, Boston, MA, 1996, p. 90.

[2]Gaonkar, G. H., and Peters, D. A., "A Review of Dynamic Inflow Modeling for Rotorcraft Flight Dynamics," *Vertica*, Vol. 12, No. 3, 1988, pp. 213–242.

[3]Krothapalli, K. R., Prasad, J. V. R., and Peters, D. A., "Helicopter Rotor Dynamic Inflow Modeling for Maneuvring Flight," *Journal of the American Helicopter Society*, Vol. 46, No. 2, 2000, pp. 129–139.

[4]Chen, R. T. N., "A Survey of Non-Uniform Inflow Models for Rotorcraft Flight Dynamics and Control Applications," *Vertica*, Vol. 14, No. 2, 1990, pp. 147–184.

[5]Brown, R. E., "Rotor Wake Modeling for Flight Dynamic Simulation of Helicopters," *AIAA Journal*, Vol. 38, No. 1, 2000, pp. 57–63.

[6]Theodore, C., and Celi, R., "Flight Dynamic Simulation of Hingeless Rotor Helicopters Including a Maneuvering Free Wake Model," *Proceedings of the American Helicopter Society 54th Annual Forum*, American Helicopter Society, Alexandria, VA, 1998.

[7]Leishman, J. G., *Principles of Helicopter Aerodynamics*, Cambridge Univ. Press, Cambridge, 2001, pp. 443–477.

[8]Brown, R. E., and Houston, S. S., "Comparison of Induced Velocity Models for Helicopter Flight Mechanics," *Journal of Aircraft*, Vol. 37, No. 4, 2000, pp. 623–629.

[9]Huber, H. B., "Determination of the Autorotation Behavior of Helicopters Using the Bo105 as an Example," *Flight Mechanics of Rotorcraft*, German Society for Aeronautics and Astronautics, 1971, pp. 39–71.

[10]Houston, S. S., "Modeling and Analysis of Helicopter Flight Mechanics in Autorotation," *Journal of Aircraft*, Vol. 40, No. 4, 2003, pp. 675–682.

[11]Houston, S. S., "Validation of a Rotorcraft Mathematical Model for Autogyro Simulation," *Journal of Aircraft*, Vol. 37, No. 3, 2000, pp. 203–209.

[12]Spathopoulos, V. M., "The Assessment of a Rotorcraft Simulation Model in Autorotation by Means of Flight Testing a Light Gyroplane," Ph.D. Dissertation, Dept. of Aerospace Engineering, Univ. of Glasgow, Scotland, U.K., Aug. 2001.

[13]Peters, D. A., and HaQuang, N., "Dynamic Inflow for Practical Applications," *Journal of the American Helicopter Society*, Vol. 33, No. 4, 1988, pp. 64–68.

[14]Toro, E. F., "A Weighted Average Flux Method for Hyperbolic Conservation Laws," *Proceedings of the Royal Society of London, Series A: Mathematical and Physical Sciences*, Vol. 423, No. 1864, 1989, pp. 401–418.

[15]Houston, S. S., "Validation of a Non-Linear Individual Blade Rotorcraft Flight Dynamics Model Using a Perturbation Method," *The Aeronautical Journal*, Vol. 98, No. 977, 1994, pp. 260–266.

[16]"14 Code of Federal Regulations Aeronautics and Space Chapter I. Federal Aviation Administration, Department of Transportation Subchapter C—Aircraft Part 27—Airworthiness Standards: Normal Category Rotorcraft," Sec. 27.173, Sec. 27.175, Sept. 1999.

[17]"14 Code of Federal Regulations Aeronautics and Space Chapter I. Federal Aviation Administration, Department of Transportation Subchapter C—Aircraft Part 29—Airworthiness Standards: Transport Category Rotorcraft," Sec. 27.173, Sec. 27.175, Sept. 1999.

[18]"ADS-33E-PRF Handling Qualities Requirements for Military Rotorcraft," United States Army Aviation and Missile Command, Aviation Engineering Directorate, Redstone Arsenal, Alabama, March 2000.

[19]Turnour, S. R., and Celi, R., "Modelling of Flexible Rotor Blades for Helicopter Flight Dynamics Applications," *Journal of the American Helicopter Society*, Vol. 41, No. 1, 1996, pp. 52–61.